Applied Catalysis B: Environmental 130–131 (2013) 168–177

Contents lists available at SciVerse ScienceDirect

Applied Catalysis B: Environmental

journal homepage: www.elsevier.com/locate/apcatb

Olivine as tar removal catalyst in biomass gasification: Catalyst dynamics under model conditions

Hans O.A. Fredriksson*, Remco J. Lancee, Peter C. Thüne, Hubert J. Veringa, J.W. (Hans) Niemantsverdriet**

Department of Chemical Engineering and Chemistry, Eindhoven University of Technology, P.O. Box 513, 5600 MB Eindhoven, The Netherlands

ARTICLE INFO

Article history:
Received 26 July 2012
Received in revised form 10 October 2012
Accepted 14 October 2012
Available online 29 October 2012

Keywords:
Biomass
Gasification
Catalyst stability
Tar
Olivine

ABSTRACT

Olivine ($(Mg,Fe)_2SiO_4$) has been extensively explored as an active bed material for catalytic cracking of tars during gasification of biomass in dual fluidized bed reactors. It is known that both the elemental composition, addition of Fe and high temperature calcinations influence the catalytic properties of this mineral. However, it is not clear how olivine responds to the fairly hostile environments present during gasification or what chemical state Fe takes during operation. We have investigated the stability of Austrian olivine under model conditions, resembling those in a gasifier. Powder samples were heated to 750 °C in a quartz-tube flow-reactor and sequentially exposed to oxidizing (O_2, H_2O, CO_2) or reducing gases (CO, H_2) or mixtures thereof, for various durations of time. Significant changes in phase composition of the material, depending on the gas composition and the duration of the treatments, were found using X-ray photo-electron spectroscopy (XPS), X-ray diffraction (XRD), X-ray absorption spectroscopy (XAS) and scanning electron microscopy (SEM). A large fraction of the Fe in the investigated material is present as free Fe-phases, which are sensitive to changes in the gas environment. After exposure to oxidizing gases, the free Fe phases are: Fe_2O_3 and Fe_3O_4 or $MgFe_2O_4$. Upon exposure to reducing gases, the iron oxides are converted into Fe^0 and Fe_3C and formation of graphitic carbon is observed. In addition, the elemental composition of the surface changes dramatically depending on the gas composition. After exposure to oxidizing environments, the amount of Fe at the surface is twice as high as after reduction. Both the change in chemical state of the Fe-phases, the amount of surface Fe and the build-up of surface carbon are fast processes under the applied conditions and significant changes are observed on the time scale of one minute. These observations have important implications for olivine as a tar cracking catalyst, especially when used in dual fluidized bed gasifiers. The fast reduction of the iron oxides upon switching from oxidizing to reducing conditions shows that olivine transports oxygen from the combustor into the gasifier. Furthermore, the catalytic properties of Fe depend strongly on its chemical state. Therefore, the catalytic function of olivine depends strongly on the gas environment and on the catalysts residence time in the gasifier. Finally, both the decreasing amount of surface-Fe and the carbon deposition observed after exposing olivine to reducing conditions can result in significant catalyst deactivation.

1. Introduction

Gasification in fluidized bed reactors is one of the preferred routes for converting biomass into useful, sustainable and CO_2 neutral fuels. An attractive feature with biomass gasification is that the resulting primary products, CO, H_2, CO_2 and CH_4 can easily be integrated with present infrastructure. Technology for converting CO and H_2 into conventional fuels, such as diesel or substitute natural gas, is already at hand, as well as an extensive distribution system for natural gas.

In a conventional fluidized bed reactor, gasification and partial combustion take place in the same chamber. Therefore, if air is used as gasification medium, the product gas contains both CO_2 and N_2, requiring a costly separation process. This can be avoided by using a dual fluidized bed reactor [1,2], where gasification takes place in the absence of air and steam is used as a gasification medium. The bed-material and the residues from the gasification process (mainly char) are then circulated into a second chamber where they are exposed to air. The resulting combustion generates heat, and the endothermic gasification process can be sustained by re-injecting the hot bed-material into the first chamber. This way, a major part of the CO_2 is conveniently separated from the product gases

* Corresponding author. Tel.: +31 40 247 3161; fax: +31 40 247 3481.
** Corresponding author. Tel.: +31 40 247 3271; fax: +31 40 247 3481.
E-mail addresses: h.o.a.fredriksson@tue.nl (H.O.A. Fredriksson), j.w.niemantsverdriet@tue.nl (J.W. Niemantsverdriet).

0926-3373/$ – see front matter © 2012 Elsevier B.V. All rights reserved.
http://dx.doi.org/10.1016/j.apcatb.2012.10.017

(allowing for sequestration) and contamination by N_2 and nitrogen-containing species is avoided. However, tar-formation, resulting from incomplete conversion of the biomass, still constitutes a major obstacle in the way of realizing competitive, large scale production of fuels from biomass. Condensation of tars leads to contamination and clogging of the reactor and subsequent pipes, eventually causing malfunction of the system. By using a catalytically active bed material, it has been shown that the tar concentration in the product gas can be decreased [3–6].

A catalytic bed material needs to be non-toxic, cheap and attrition resistant. A widely used and investigated candidate is the naturally occurring mineral olivine ($(Mg,Fe)_2SiO_4$) [1,4,7–11]. Although this material has proven active for tar reduction, the underlying catalytic mechanism is not clear. Furthermore, the exact nature of the material under operational conditions is unknown, making optimization of the catalyst and the process conditions difficult. Previous work points at Fe as the catalytically active component in olivine as well as in other Fe-containing materials [3,12,13]. However, at the temperatures typically applied during gasification (between 700 and 1000 °C) olivine is only thermodynamically stable in gas compositions with partial oxygen pressures within a fairly narrow interval [14] (note that even gases that are nominally oxygen-free may have a partial pressure of oxygen due to chemical equilibrium reactions). It is therefore expected, both from theory and from experimental work, that the mineral is subject to significant changes under gasification conditions.

In this work we aim at clarifying the changes in phase composition of olivine upon exposure to the gases present during gasification of biomass at relevant temperatures and for various durations. We study a naturally occurring olivine, previously shown suitable as catalytic bed material [4,8,10,11]. Exposure to gases is done in a quartz-tube flow-reactor with good control over gas environment and process temperature.

2. Experimental

2.1. Materials

Olivine from Magnolithe, Austria was used in all experiments. A 3 h, 1600 °C calcination of the material was performed by the mineral supplier. The grain size during this pre-calcination was on the order of 10 mm. Prior to experiments the olivine was grinded or ball milled to a powder. The grain diameters are on the order of a few tens of or a few micrometers in diameter respectively, as estimated from scanning electron microscopy (SEM) images. The specific surface area of the powders, as determined from nitrogen sorption isotherms, was 0.53 m^2/g and 0.8 m^2/g for the grinded and the ball-milled samples respectively. The larger, grinded particles (0.1 g of sample material per experiment) were used in the experiments analyzed by SEM and X-ray photo-electron spectroscopy (XPS) and the ball-milled olivine powder (1 g per experiment) was used for the experiments analyzed by X-ray diffraction (XRD) and X-ray absorption spectroscopy (XAS).

2.2. Treatments

All treatments of the catalytic olivine powders were performed in a quartz-tube flow-reactor at 750 °C. The gases used were pure Ar, H_2, CO, CO_2 and Ar/O_2 80/20 vol.% mixture. Total flows were set to 200 ml/min. Water was added to the gas streams by passing the gas-mixtures through a bubbler containing de-ionized water, resulting in a water content of 3.5 vol.% at room temperature, as determined by a Mitchell instruments, MDM300 advanced dew-point hygrometer. In all experiments, the samples were first heated to 750 °C under Ar flow. At this temperature, the gas flow was switched to the reactive gas mixtures for a specified time. After the treatment, the gas mixture was switched back to Ar and the flow reactor quickly cooled to room temperature.

2.3. Characterization

All characterizations were performed ex situ, after transfer of the powders under ambient conditions from the quartz tube flow reactor.

S_{BET}: Nitrogen sorption isotherms were measured at −196 °C using a Micromeritics tristar II 3020, after outgasing the samples for 3 h at 180 °C. The Brunauer–Emmett–Teller (BET) equation was used to calculate the specific surface area (S_{BET}).

SEM: A FEI Quanta 3D FEG dual beam was used for the SEM characterizations.

XRD: XRD spectra were taken using a Bruker D4 Endeavor powder spectrometer using Cu Kα radiation and a scan speed of 0.009 min^{-1}. After the high temperature treatments the olivine powders were mixed with 6% of pure NaCl for accurate calibration of the peak positions. The XRD-references and their respective ICDD-file numbers used where; $(Mg,Fe)_2SiO_4$ #71-1080, ($MgSiO_3$) #35-610 and 19-606, α-Fe_2O_3 #71-5088, γ-Fe_2O_3 #39-1346, Fe_3O_4 #71-6336, $MgFe_2O_4$ #17-464, FeO #89-687, α-Fe #65-4899, Fe_3C #35-772, graphite #75-1621, MgO #4-829, NaCl #75-306.

XAS: XAS-measurements were performed at the Advanced Photon Source of The Argonne National Laboratory. The energy was scanned over the Fe K edge and grazing incidence fluorescence mode was used.

XPS: XPS-spectra were taken using a Kratos Axis Ultra and a Thermo scientific K-alpha spectrometer with monochromatic Al Kα sources. Analysis and quantification of the measurements was performed using the Casa-XPS software and Wagner sensitivity factors [15]. Charge neutralization was always used and the spectral position adjusted to the Si2s peak of olivine at 153 eV [16]. For quantification the Mg2p, Fe3p, Si2s, C1s and O1s signals were used.

3. Results

The experiments presented in this paper are divided into two sections. The focus in both sections is on investigating the dynamic behavior of olivine exposed to the gases that are present in a typical biomass gasification reactor. In particular, we present results investigating how the phase composition and morphology of the material changes upon entering the gasification zone from the combustor. The experiments described in the first section were done to investigate long-term behavior (hours) of olivine, i.e. what happens to the catalyst after extended exposure to the gases present in a gasification reactor. In the second section we focus on the short-term dynamics of the material, i.e. the materials behavior on time scales of one to a few tens of minutes. More specifically, we aim at answering the question: how fast does the surface elemental composition change in response to a change in the gas environment? All together, we are aiming at clarifying whether olivine is best thought of as a stable material or if it is a catalyst in constant transition from one configuration to another during use in a dual fluidized bed gasifier.

3.1. Long term trends

3.1.1. Long term behavior, six standard treatments, four characterization techniques

We have treated samples of grinded or ball-milled olivine powders in a quartz-tube flow-reactor in various gas mixtures aiming at mimicking the conditions in a dual fluidized bed reactor. The conditions in the combustion zone were accurately reproduced by flowing synthetic air (Ar/O_2, 80/20 vol.%, here after referred to as

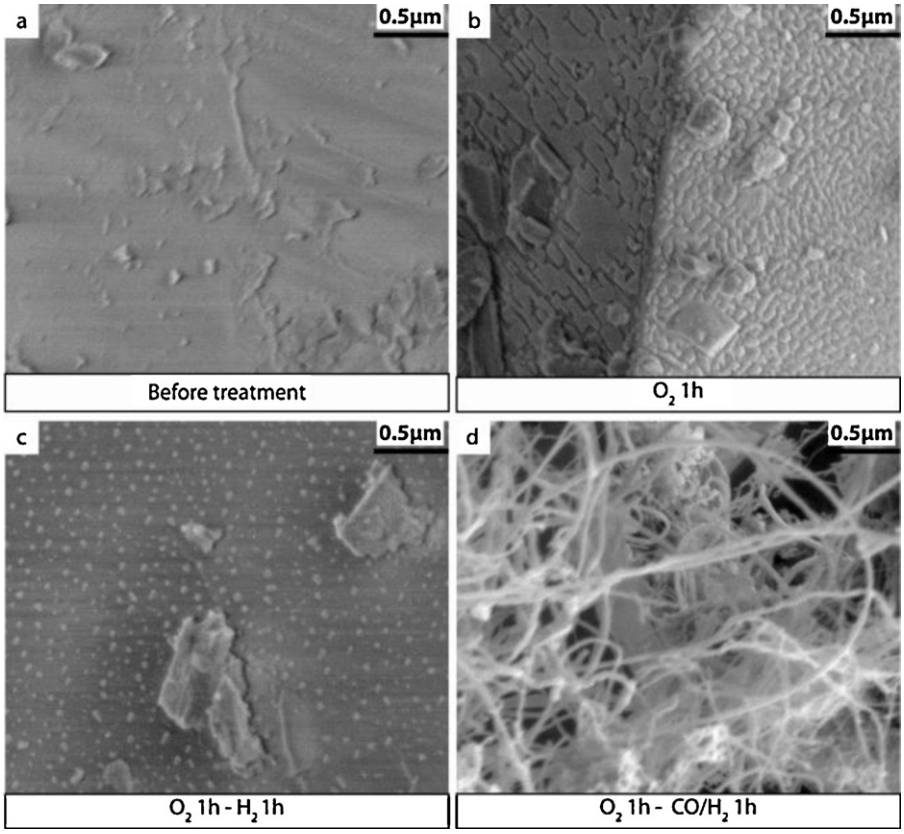

Fig. 1. SEM micrographs of olivine before (a) and after treatment at 750 °C for 1 h in oxygen (b) followed by 1 h in H_2 (c) or CO/H_2 (d).

O_2) over a thin layer of olivine powder at 750 °C for 1 h. The conditions for olivine entering the gasification zone from the combustor are somewhat more difficult to simulate since the concentration of the various gases depend on the process conditions as well as on the quality of the biomass and the residence time. Furthermore, the environment that the catalyst is exposed to in the gasification zone is not homogeneous since biomass and steam are gradually converted into products gases. Therefore we exposed olivine, first to synthetic air for 1 h as above, and subsequently to the product gases CO and H_2, either separately or in 50/50 vol.% mixtures, for another hour. Since water is one of the other main constituents of the gas mixture in the gasification zone, we also exposed 1 h pre-oxidized olivine to water saturated Ar and syngas by passing the gas streams through a water bubbler. In total seven samples were examined for the long-term behavior. One of them was left untreated and the six remaining samples were treated at 750 °C for 1 h in O_2. Five of the oxygen-treated samples were subsequently treated for another hour (750 °C) in mixtures of Ar, H_2, CO and H_2O, as described in Table 1. Samples subjected to these treatments were then characterized using SEM, XRD, XAS and XPS.

Fig. 1 shows the most interesting SEM micrographs of surfaces of un-treated, oxidized and reduced olivine. The surface of the untreated olivine (Fig. 1a) is smooth and flat whereas oxidation for 1 h results in the formation of crystallites (Fig. 1b). Olivine that has been exposed to water or H_2 after the oxidation still shows crystallites at the surface, but less pronounced. Especially for the H_2-reduced olivine, the crystallites are substantially smaller and rounder (Fig. 1c). The three samples exposed to CO-containing gases after oxidation all show deposition of material on the surface. The fibrous structure of the deposited material suggests that it consist of carbon fibers (Fig. 1d).

Fig. 2 shows the XRD spectra of seven ball-milled olivine powder samples after the treatments described above. The diffraction peaks of olivine and the strongest peaks of the relevant minority phases observed in the spectra are indicated. All spectra have been normalized to the main diffraction peak of olivine at $2\theta = 36.5°$.

It is clear that the main crystalline constituent in all of these samples is olivine. The other crystalline phase that is present in all the samples, regardless of treatment, is pyroxene ($MgSiO_3$). It is also clear from these measurements that the other crystalline phases that form during oxidation and reduction are various iron compounds, graphite and magnesium oxide. This is illustrated in Fig. 3, where close-ups on the regions of interest are shown, with the position of the strongest diffraction line of the formed phases indicated.

Fig. 3c shows that the material contains a significant fraction of one or both of the indistinguishable spinel phases Fe_3O_4 and $MgFe_2O_4$, even before any high temperature treatment is applied. After treatment in O_2 an additional hematite (α-Fe_2O_3) phase evolves (Fig. 3c). For the case where the O_2 treatment is followed

Table 1
Names of the samples presented in the figures in Section 3.1 and details of the treatment sequences.

Name in figures	1 h, 750 °C, gas flow	1 h, 750 °C, gas flows
Before treat.	Not applied	Not applied
O_2	Ar/O_2 200 ml/min	Not applied
O_2–H_2O	Ar/O_2 200 ml/min	Ar 200 ml/min, 3.5 vol.% H_2O
O_2–H_2O/CO/H_2	Ar/O_2 200 ml/min	CO 100 ml/min, H_2 100 ml/min, 3.5 vol.% H_2O
O_2–CO/H_2	Ar/O_2 200 ml/min	CO 100 ml/min, H_2 100 ml/min
CO	Ar/O_2 200 ml/min	CO 200 ml/min
H_2	Ar/O_2 200 ml/min	H_2 200 ml/min

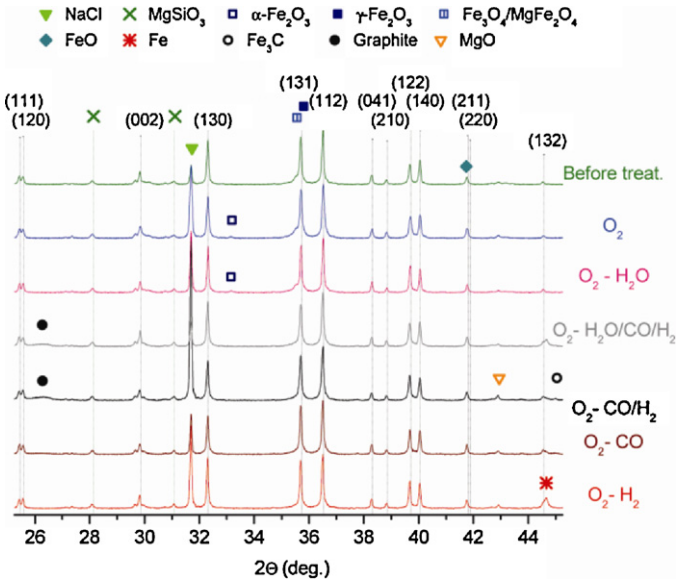

Fig. 2. XRD spectra of olivine before and after treatment at 750 °C, 1 h in oxygen followed by 1 h in various mixtures of H_2, CO and H_2O. The reflection indices of olivine are indicated together with the position of the main reflection of other phases observed in the spectra.

by a treatment in H_2O these phases remain unchanged, whereas a subsequent reducing treatment removes them completely. During reducing treatments, iron carbide (Fe_3C) and/or metallic iron (α-Fe) form (Fig. 3e) instead of the iron oxide phases that were present after the initial oxidation treatment. The iron carbide is only observed in the samples treated in CO containing gases. In addition, a distinct graphite peak can be seen in the spectra of these samples (Fig. 3a). This observation lends further support to the hypothesis that the deposits on these samples, observed in SEM (Fig. 1d), are indeed carbon fibers. Another observation worth pointing out is that there seem to be a slight increase of magnesium oxide (MgO) in samples treated in H_2 and CO/H_2.

In Fig. 4a we present XAS-spectra of olivine powders subject to the same treatments as described above. The main observations are that the treatment in O_2 and O_2 followed by H_2O leads to a shift of the main absorption edge toward higher energies. Oxidation

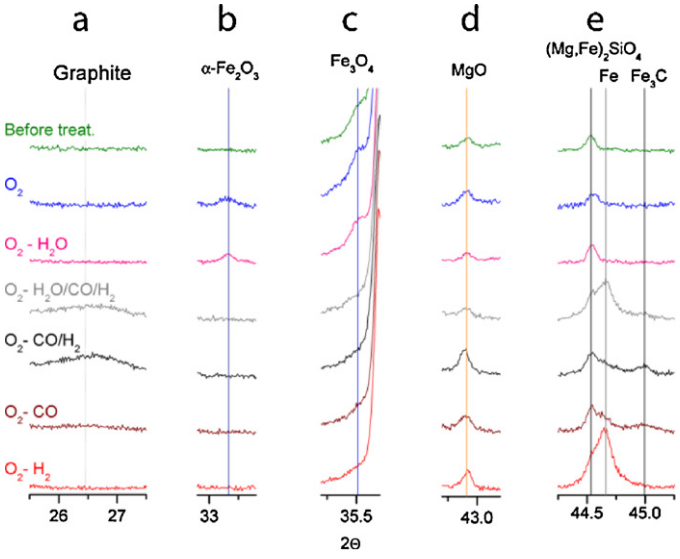

Fig. 3. Close-ups on the regions where changes are observed in the spectra displayed in Fig. 2.

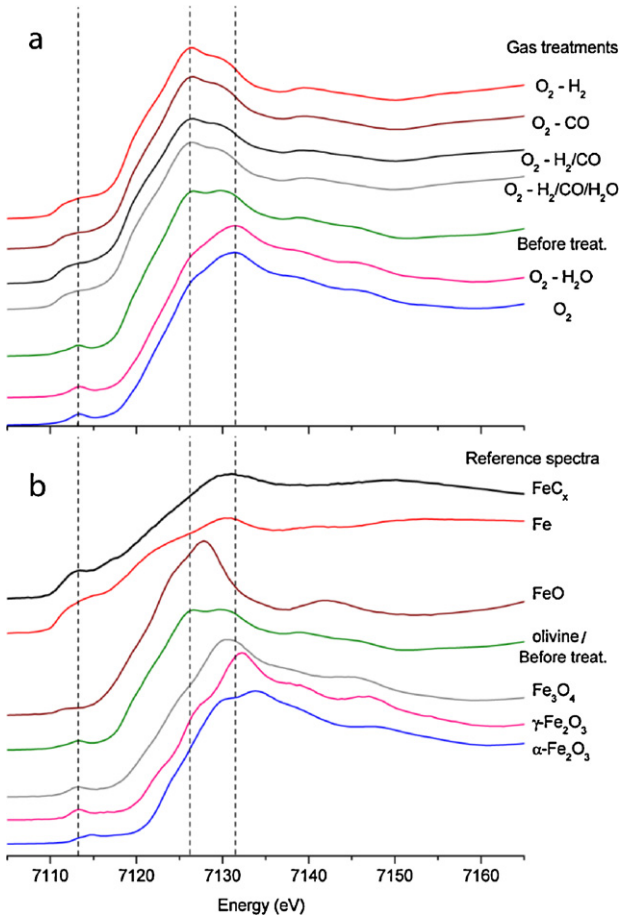

Fig. 4. (a) XAS spectra showing olivine samples before and after treatment at 750 °C, 1 h in O_2 followed by 1 h in various mixtures of H_2, CO and H_2O and (b) reference spectra of Fe-containing materials. The dashed lines have been added as a guide to the eye.

followed by reduction in H_2 and CO containing gases on the other hand leads to a shift to lower energies. Fig. 4b shows spectra of iron, iron-oxides and -carbide, presented previously in [17], for comparison. The reference spectra suggest that the shifts observed after oxidation can be interpreted as transformation of the material toward Fe_3O_4, γ-Fe_2O_3 and α-Fe_2O_3. The shifts of the olivine spectra to lower energies as a result of treatment in reducing atmospheres, on the other hand, suggests that metallic Fe, FeO and iron carbide (FeC_x) form, thus confirming the trends observed in XRD.

These trends can be clarified and quantified using linear combinations fits of the references spectra in Fig. 4b to reproduce each spectrum in Fig. 4a. The weight of each reference spectrum in the fit then corresponds to the amount of that phase present in the material after each treatment. In lack of a good, pure olivine reference, we use the "before treatment" sample to represent the original material. From our XRD measurements, it is clear that this sample contains significant quantities of $MgSiO_3$ and Fe_3O_4 or $MgFe_2O_4$. Furthermore, from the literature it is known that about 45% of the iron in the Austrian olivine (from Magnolithe, as that used in this study) persists in the form of free iron oxide phases [9]. Although the use of a non-pure reference in the linear combination fitting is not ideal, it still provides useful information on the new phases formed after the different treatments. The results are presented in Fig. 5, as change in phase content compared to the un-treated material. Positive numbers indicate that the presence of the corresponding phase has increased and vice versa.

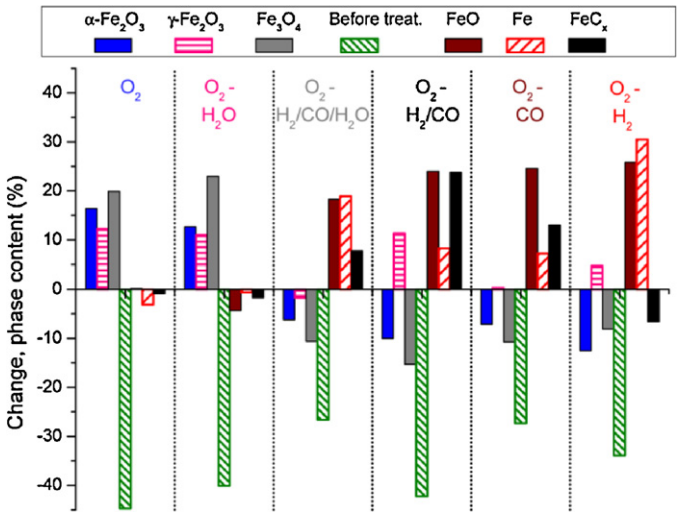

Fig. 5. Quantification of the change of the content of various Fe-phases present in olivine, before and after treatments in various gas mixtures from linear combination fitting of the spectra presented in Fig. 4.

This analysis shows that between 25 and 45% of the Fe-containing fraction, present in the original material, is affected by the treatments. Consequently the majority of this fraction remains unaffected. After treatment in oxidizing gases, the amount of iron present as Fe_3O_4, γ-Fe_2O_3 and α-Fe_2O_3 increases significantly. Oxidation for 1 h followed by 1 h under reducing conditions converts these iron oxides into metallic Fe, FeO and, if the reducing gas contains CO, into FeC_x. The largest amount of FeC_x is observed after treatment in dry syngas and the largest amount of metallic Fe is observed after treatment in hydrogen.

The surface properties of olivine powders subjected to the same oxidizing and reducing treatments as discussed above were investigated using XPS. Fig. 6 shows the normalized spectra for the four elements constituting olivine after each treatment.

These measurements show, in similarity with the previously presented XRD and XAS results, that main changes apply to the iron in the material. The Si2s peaks, on the other hand, show no significant changes and were therefore used for charge correction of the spectra using the energy previously reported for Si2s in olivine at 153 eV [16]. Likewise, no significant changes are observed in the Mg2p peak after the various treatments. In contrast, the Fe2p peak indicates several interesting surface transformations. Although it is not straightforward to exclusively identify different Fe-phases from XPS measurements, it is possible to derive the oxidation state of the material. Literature [18–20] reveals that the presence of a main $Fe2p_{3/2}$ peak at 711 eV and a satellite peak at 719 eV is characteristic for Fe^{3+} as found, e.g. in Fe_2O_3. For Fe^{2+}-containing material (as found in FeO or olivine), the corresponding main peak appear at 709 eV and the satellite at 715 eV. For reduced iron (Fe^0), the main peak is positioned at around 707 eV and there are no satellite peaks. These positions are marked with dashed lines in the figure. It is clear that an Fe^{3+}-rich phase (presumably γ-Fe_2O_3 or α-Fe_2O_3) is formed at the surface as a result of exposure to oxidizing conditions (O_2 and O_2 followed by H_2O). This is evidenced by the presence of a broad satellite peak in the Fe2p spectra around 719 eV as well as by the formation of a low-energy shoulder in the O1s spectra at 530 eV (typical for metal oxides [20]). For the olivine powders that were first oxidized for 1 h and then subjected to reducing conditions for 1 h, the 719 eV satellite has disappeared or significantly decreased, the main peak is broadened and shifted toward lower binding energies and a peak at 707 eV is observed. These observations indicate that the Fe^{3+}-phase formed during oxidation is reduced to a combination of Fe^{2+} and Fe^0-dominated iron phases, such as olivine,

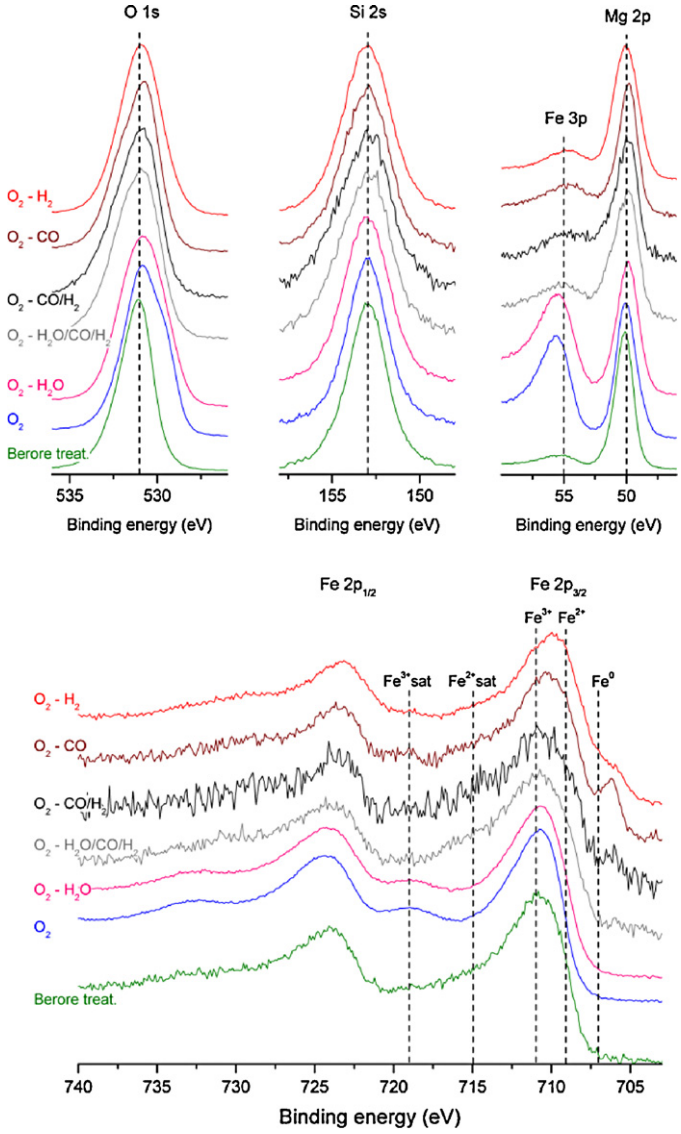

Fig. 6. XPS spectra of the elements that constitute olivine, before and after treatment at 750 °C, 1 h in oxygen followed by 1 h in various mixtures of H_2, CO and H_2O.

Fe_3O_4, FeO, α-Fe or FeC_x. Furthermore, the relative intensities of the Fe3p and Mg2p peaks indicate significant changes in the amount of Fe present at the surface. Exposure to oxidizing conditions leads to an increase of surface-Fe whereas a subsequent reduction results in levels similar to those observed before oxidation.

It should be noted that these experiments were not done in situ, i.e. the samples were exposed to air upon transfer from the treatment reactor to the XPS. Therefore, estimations based on the amplitude of the Fe^0 peak is expected to underrate the presence of metallic iron, since surface oxides are known to form rapidly at room temperature and ambient atmosphere. The higher noise levels in the spectra from samples treated in CO-containing gases derive from lower signal intensities due to substantial deposition of carbon on the surface. We will return to this in the following sections.

3.1.2. *Intermediate gas compositions*

To investigate the changes in surface composition as a result of exposure to gases with different oxidizing power in greater detail, various mixtures of CO_2/CO were used. By changing the relative

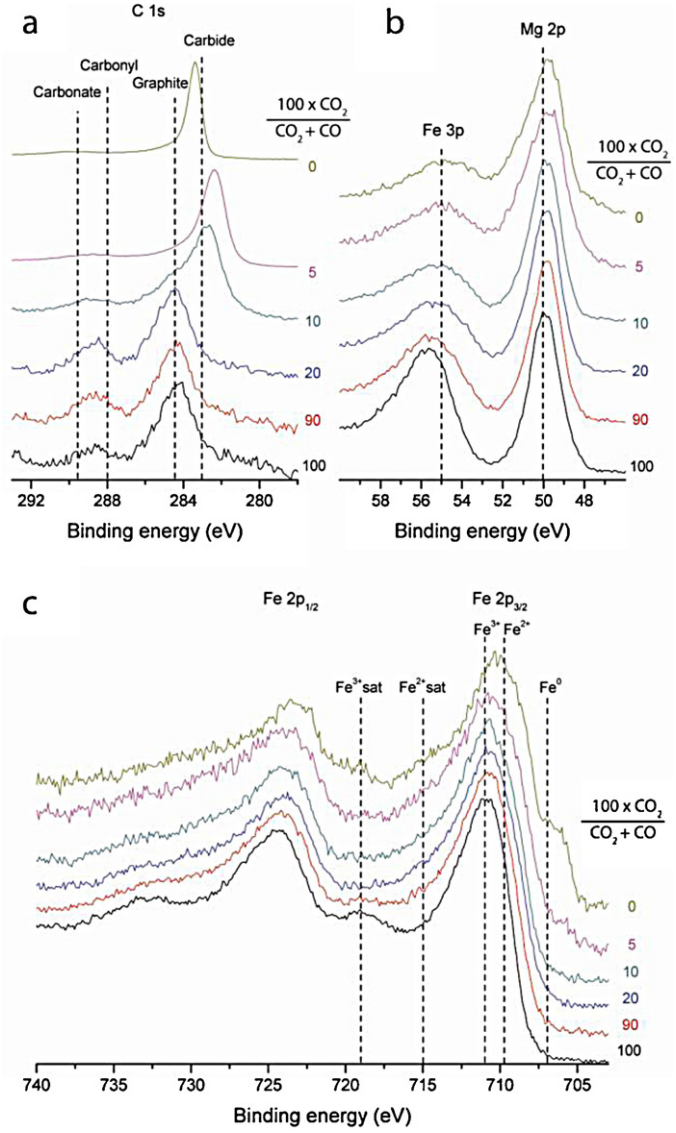

Fig. 7. XPS spectra from samples treated at 750 °C in O_2 for 1 h followed by 1 h in CO_2/CO mixtures with CO_2 contents of 0, 5, 10, 20, 90 and 100 vol.%.

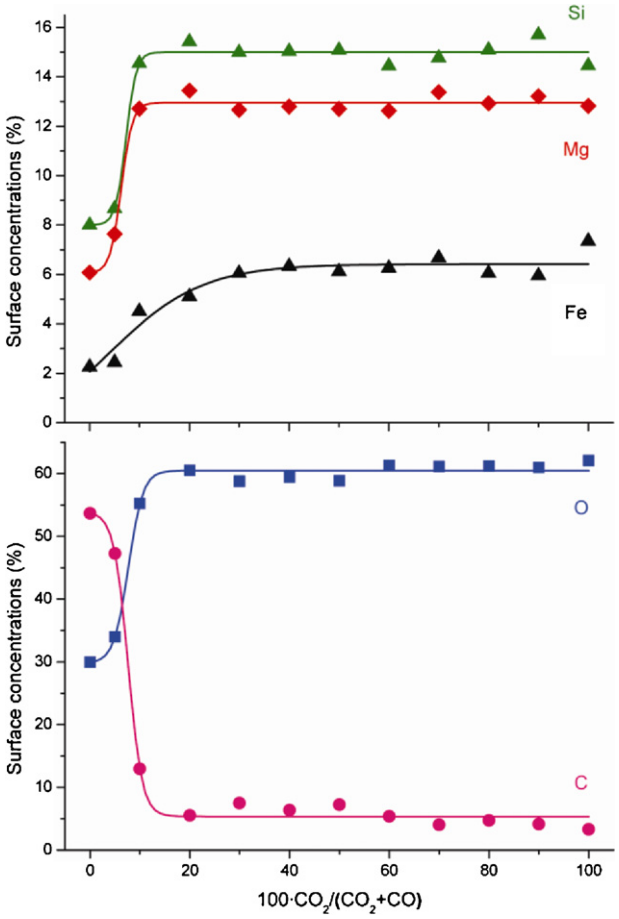

Fig. 8. Quantification of the XPS-derived elemental composition of the olivine surface after treatment at 750 °C in O_2 for 1 h followed by 1 h in various mixtures of CO_2 and CO ranging from 0 to 100 vol.% CO_2. The lines are sigmoidal fits serving as guides to the eye.

content of the two gases, the oxygen content in the gas can be fine-tuned via the equilibrium reaction

$$CO + 0.5O_2 \Leftrightarrow CO_2 \quad (1)$$

Fig. 7 shows normalized C1s, Fe3p/Mg2p and Fe2p peaks for olivine powders that were first exposed to O_2 for 1 h followed by 1 h in different CO_2/CO gas mixtures with CO_2 contents ranging from 0 to 100 vol.%.

After treatment in pure CO_2 the material remains oxidized, exhibiting spectra resembling those after exposure only to O_2 (see Fig. 6). However, already after including 10 vol.% CO in the gas mixture, the Fe^{3+} is reduced to Fe^{2+}, as seen by the decreasing intensity of the Fe2p satellite peak at 719 eV. Very little happens to the material when the CO_2 content is decreased further down to 20 vol.% (spectra for concentrations in between not shown), whereas below this concentration the peak at 707 eV, characteristic for metallic iron (Fe^0) or iron carbide, slowly starts to grow. A decrease in the Fe3p/Mg2p ratio is also observed as the CO_2 content is reduced, indicating a decrease of the iron content at the surface. For samples treated in CO_2-rich gas mixtures the C1s peak is small and representative for carbon species naturally introduced to the sample by exposure to airborne contaminants during transfer from the quartz tube reactor to the XPS chamber. However, when the CO_2 content of the gas mixture is decreased to 10 vol.% a new carbon peak, typical for carbides [20], starts to grow at around 283 eV. For even lower CO_2 contents the carbon peak amplitude grows significantly and for pure CO a shift of the peak to higher energy is observed. We have seen in the previous sections that both iron carbide and graphitic carbon forms on the sample surface after treatment in pure CO. However, repeated measurements of samples subjected to the same treatments show that the position of the carbon peak varies significantly between nominally identical samples. This is likely due to differential charging of the conducting carbon layer deposited on the insulating olivine; C1s spectra of samples with thick carbon over-layers should therefore be interpreted with caution.

The elemental surface composition of the powders exposed to the various CO_2–CO mixtures, calculated from the XPS-data, is presented in Fig. 8.

The quantification clearly demonstrates that the most significant changes of the surface elemental composition take place when the CO_2 content of the gas mixture is decreased to 20 vol.% or below. At 20 vol.% CO_2 content, there is first a small decrease in the Fe content at the surface and in more CO_2 deficient gas mixtures a significant build-up of carbon on the surface is observed.

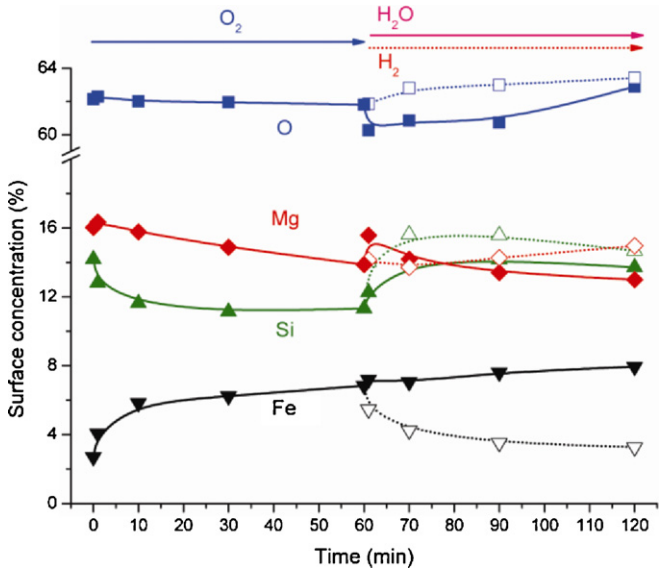

Fig. 9. Surface elemental composition of olivine measured with XPS. The material was first exposed to O_2 and then to H_2 (open symbols, dashed lines) or H_2O (solid symbols, solid lines). Each measurement point refers to a separate sample subject to the treatment up to that point.

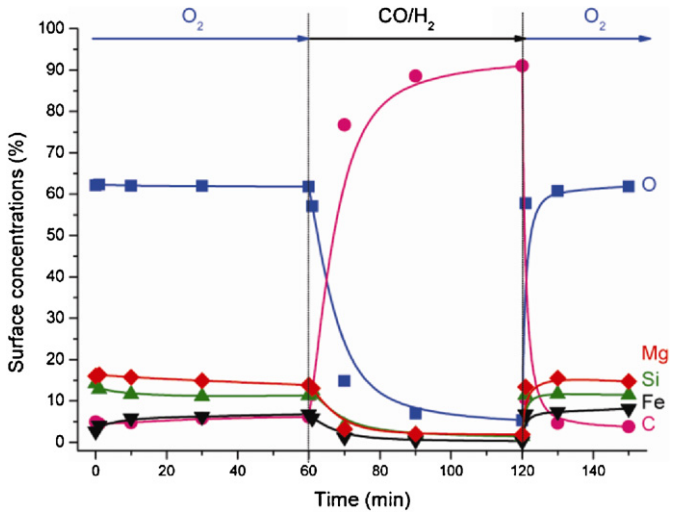

Fig. 10. Surface elemental composition of olivine measured with XPS. The material was first exposed to O_2 and then to a 50/50 mixture of CO and H_2 and finally to O_2 again. Each measurement point refers to a separate sample, subjected to the treatment up to that point.

3.2. Time-dynamics of the surface elemental composition

In order to elucidate the dynamic behavior of olivine in different gas environments, we exposed fresh, grinded material to well defined gas environments at 750 °C for various durations and analyzed the surface elemental composition after each time-interval using XPS. Fig. 9 shows olivine, first exposed to O_2 for durations up to 1 h and subsequently exposed to H_2 or H_2O for time durations up to 1 h.

The key observations are the following: (i) upon exposure to O_2, simulating the catalysts presence in a combustion chamber, the amount of iron at the surface increases, initially at the expense of Si and in the longer run at the expense of Mg. (ii) Switching gas environment from O_2 to H_2 reverses this process, i.e. the iron surface content decreases and is initially replaced by Si, and after a longer duration of time, also by Mg. (iii) Switching from O_2 to H_2O, the iron content at the surface is maintained. (iv) The surface content of iron is roughly twice as high under oxidizing conditions (O_2 or H_2O) as under reducing conditions (H_2) and (v) the changes in surface elemental composition happen fast and are significant already after one minute. This is true also for the change in chemical state of the surface iron, which goes from the fully oxidized hematite state to the reduced state already after the first minute under reducing conditions.

The exposure of oxidized olivine to H_2 and H_2O serves to simulate the exposure of the catalyst material to the conditions in the gasification zone. However, in the gasification zone, the catalyst is exposed to carbon-containing gases (as well as to the biomass itself), which result in significant changes in the olivine, as demonstrated in previous sections. Fig. 10 shows a similar sequence of measurements as in Fig. 9, but where the oxidation treatment is followed by reduction in syngas and that ends with an oxygen treatment.

Again, the surface content of iron increases during oxidizing conditions and decreases under reducing conditions. However, the most striking feature observed from these measurements is the build-up of carbon on the surface during exposure to syngas. Before exposure to carbon-containing gas, between 4.5 and 6.1% of carbon is observed on the surface of the catalyst. These small quantities of carbon are expected, as a result of the contact with atmospheric contaminants during transfer from the treatment reactor to the XPS. However, after a one-minute exposure to syngas, the amount of carbon on the surface is roughly doubled (11.5%) and after an hour carbon constitutes more than 90% of the surface atoms. This carbon layer is then quickly combusted when the sample is exposed to oxygen. A similar build-up of carbon on the olivine surface is observed for the other CO-containing mixes (not shown), and is most significant for the case of pure syn-gas, somewhat slower in wet syn-gas and slower yet in pure CO.

To further investigate and emphasize the dynamics of the olivine exposed to alternating gas environments on time scales relevant in a dual fluidized bed reactor, we performed experiments with short pulses of alternating oxidizing and reducing gas. The samples were exposed to oxygen for one minute, oxygen was then purged out with Ar for one minute followed by exposure to CO for one minute and another minute of Ar purging. This four-minute cycle was repeated up to 10 times and the response of olivine after various numbers of cycles (or fraction of cycles) is shown in Fig. 11.

These measurements show that the material readily responds to the changing gas environments on the short time-scales of a treatment cycle. After the oxidation step in each cycle, the amount of iron at the surface increases significantly on the expense of Si whereas the opposite is true after the reduction steps. Superimposed on this effect is a slower response in which the amount of iron at the surface increases on the expense of magnesium. Furthermore, no accumulation of carbon on the surface is observed after repeated cycles although there is generally more carbon present after a CO step than after an O_2 step as expected.

4. Discussion

The experiments presented above demonstrate that olivine is a very dynamic material under conditions typical for biomass gasification. Changes in the gas composition at relevant temperatures result in a fast response in the chemical state of the material. These changes predominantly concern the Fe present in the material.

4.1. Iron

The XRD measurements (see Figs. 2 and 3) show that the Austrian olivine contains a significant fraction of the crystalline spinel phase (Fe_3O_4 or $MgFe_2O_4$), even before we apply any

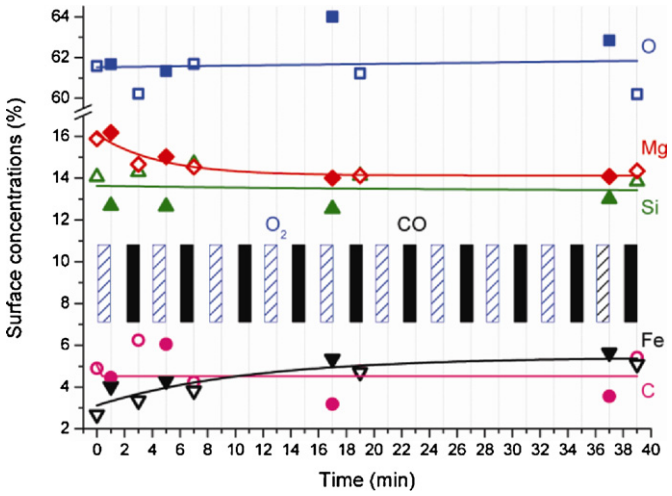

Fig. 11. Surface elemental composition of olivine measured with XPS after various numbers of alternating O_2–CO cycles at 750 °C. Solid symbols represent measurements done after an O_2 step in a cycle and open symbols the material after a CO step. The solid, black rectangles in the background mark the time where the samples were exposed to CO and the blue, striped rectangles mark where there was an O_2 flow. The solid lines are exponential fits to the data, serving as guides to the eye. (For interpretation of the references to color in this figure legend, the reader is referred to the web version of the article.)

high temperature treatments. This is in agreement with previous studies [9,10], where Mössbauer spectroscopy showed that almost half of the iron in olivine (of the same origin as that studied here) is present in the form of free oxides, predominantly $MgFe_2O_4$ and non-crystalline α-Fe_2O_3. The presence of these free Fe-phases stems from exclusion of Fe from the olivine matrix during the pre-treatment done by the mineral supplier.

XRD and XAS (Figs. 2–5) show that oxidation of the material at 750 °C in O_2 for 1 h results in formation of the Fe^{3+}-rich phases: α-Fe_2O_3, γ-Fe_2O_3, and Fe_3O_4 and/or $MgFe_2O_4$, the latter two henceforth referred to as spinel. The XRD measurements show clearly the formation of crystalline α-Fe_2O_3 while the XAS measurements indicate the formation of γ-Fe_2O_3 and spinel as well. This discrepancy can stem from the fact that both γ-Fe_2O_3 and spinel XRD-spectra overlap significantly with the main peaks of olivine and that small changes therefore are hard to detect. Indeed, the elemental composition of our olivine can be expressed as $(Mg_{0.93}, Fe_{0.07})_2SiO_4$ [9], indicating that the vast majority of the material is actually constituted of pure Mg_2SiO_4, with no inclusion of Fe. Therefore, even a total conversion, from one Fe-containing phase to another, would come through as a relatively small change in the XRD measurements. In XAS, on the other hand, only the Fe in the material contributes to the measurement and the material does not have to be crystalline. Therefore, the latter technique is sensitive even to minor changes in the Fe-carrying phases and detects changes also in amorphous material.

Subsequent treatment of the oxidized olivine in H_2O-saturated Ar for 1 h at 750 °C shows no significant change in the Fe-phases. A similar treatment in reducing gases, on the other hand, results in a clear decrease of the Fe^{3+}-rich phase content. Both XRD and XAS show that these phases are converted to metallic Fe and, if the reducing gas contains CO, to iron carbide. In addition, the XAS measurements suggest the formation of FeO, which is not seen in XRD, likely for the same reasons already discussed above. Both techniques show that the formation of metallic Fe is most pronounced after treatment in H_2. Iron carbide formation, on the other hand, is most efficient upon treatment in dry syngas.

These measurements show that the main change in the material upon exposure to oxidizing or reducing gases is simply conversion of the Fe already excluded from the olivine matrix, e.g. conversion of iron oxides to metallic iron and/or carbide upon reduction. However, both the XRD- and XAS-measurements indicate that additional free Fe-phases are formed during these treatments, a somewhat surprising result considering the low temperatures applied. The XAS data in particular suggest that the observed Fe-phases are formed at the expense of the original Fe-carrying material, which consist at least to 50% of olivine and pyroxene. The 26–45% decrease of the original material content, suggest that another 13–22.5% of the Fe is converted from the olivine or pyroxene phases into other iron phases. The formation of free Fe-phases from olivine is in accordance with thermodynamic calculations [14] showing that olivine is only stable in a fairly narrow range of oxygen partial pressures termed the stability field. For gas environments with a higher oxygen partial pressure, olivine is expected to decompose into SiO_2, $MgSiO_3$ and Fe_3O_4. At oxygen contents below the stability field of olivine, decomposition to SiO_2, $MgSiO_3$ and Fe^0 is expected. Under oxidizing conditions corresponding to air, Fe_2O_3 is expected to form from Fe_3O_4, whereas reduction in H_2, CO or mixes thereof is expected to result in the formation of metallic Fe and FeC respectively [13,21]. Thus, in all our measurements olivine and the free Fe-phases behave in accordance with thermodynamic predictions. However, we do not observe any SiO_2 in our XRD measurements indicating that the Fe exclusion leaves behind an amorphous SiO_2 component.

Thermodynamics determines what or which of the mineral phases that are stable in a certain gas environment. Therefore, changes in the gas composition are expected to lead to changes in the material. These changes should be most significant at the surface of the material, where the material is directly exposed to the gases. Indeed, XPS (see Fig. 6) characterization of the materials surface reveals the same trends as observed by the bulk techniques XRD and XAS. After treatment in oxidizing environment, the Fe is oxidized to a Fe^{3+} type of material. Under the conditions applied here, this phase should be α-Fe_2O_3, as also observed by XRD. After treatment in reducing gases, the Fe^{3+} is reduced to a combination of Fe^{2+} and Fe^0. The Fe^0 is characteristic for metallic Fe or FeC, while the Fe^{2+} is the signature of a Fe_3O_4, FeO or olivine [16,18–20]. Upon exposure to air at room temperature, reduced Fe is quickly oxidized to form a thin surface oxide layer. Therefore, since our high-temperature treatments were done ex situ, we expect to see an oxidized surface layer, also on the reduced samples. Since we still observe a significant contribution from Fe^0 in our XPS-measurements and since large amounts of metallic Fe and FeC are observed with XRD, it is fair to assume that the surface was completely reduced during treatment, but re-oxidized during transfer to the XPS-chamber.

Another important observation from the XPS measurements (see Figs. 6–11) is that the amount of Fe at the surface of the olivine increases after oxidizing treatment. This has been reported previously [12,22] as a consequence of treatments at 900 °C for 1 h or longer and was then interpreted as surface enrichment of Fe at the expense of Mg or due to redistribution of the surface Fe. However, by investigating also the short term behavior (see Figs. 9 and 11), we have found that the Fe enrichment at the surface takes place on two time scales; a fast response on the time scale of one minute and a slower response, on the time scale of 20 min to 1 h. On the short-time scale the amount of surface-Fe increases at the expense of Si whereas on the longer time scale, Fe increases at the expense of Mg. Upon switching from oxidizing to reducing conditions, the trends are reversed, i.e. the Fe surface concentration decreases first quickly, re-exposing Si and then continues to decrease more slowly, re-exposing Mg. It should also be mentioned that the oxidation-state of the surface-Fe changes from the Fe^{3+} dominated state (observed after oxidation) to the Fe^{2+}/Fe^0

state (observed after reduction), already during the first minute after switching gases.

The long-term change in surface elemental composition is consistent with an enrichment mechanism due to diffusive exchange of Fe- with Mg-atoms at the surface of olivine, as suggested in the previous work [12]. The short-term behavior, however, is not likely due to diffusion, which is a slow process at these temperatures [23,24]. A tentative explanation for the short-term change in surface concentration of Fe can instead be provided by considering the following: it is known that natural minerals in general, including olivine, are not perfectly homogeneous materials on the microscale [25,26]. It is also known that almost half of the Fe in the olivine, investigated in this study, is present in the form of free Fe-phases [9,10]. Furthermore, Fe is more likely to segregate out of Fe-rich olivines, since Fe-diffusion is faster in these domains and since the stability field for Fe-rich olivine is narrower than that of Mg-rich olivines [14,24,27]. Free Fe-phases are known to form hematite crystallites at the surface of olivine upon oxidation [25,28–30] in agreement with what we see in SEM (see Fig. 1d). Assuming that Fe has segregated out predominantly from Fe rich domains in the olivine, we have a situation where Fe-particles are supported on amorphous SiO_2. Since the volume of Fe-particles increases upon oxidation and decreases upon reduction, this would lead to the observed effect with a fast increase of the Fe signal on the expense of Si, as observed here. It is also important to note that the amount of surface-Fe changes reversibly (or increases slightly) after repeated oxidation–reduction cycles (Fig. 11), indicating that no sintering of the free Fe occurs.

The experiments discussed so far were all done using mixtures of the gases that are present in a biomass gasifier. While the conditions in a combustor are accurately simulated by the oxidation in Ar/O_2 the other gas mixtures are not reproducing the conditions during gasification as accurately. These are rather somewhere in-between the oxidizing environment of H_2O-saturated Ar and the reducing mixtures of H_2, CO and H_2O. This interval of intermediately oxidizing gas-mixtures was investigated through the experiments with CO_2/CO mixtures (Figs. 7 and 8). It was seen that for the majority of CO_2/CO mixtures (20–90 vol.% CO_2) the surface-Fe was neither in the completely oxidized Fe_2O_3 state nor the reduced Fe^0 state, but in an intermediate state. This state is dominated by Fe^{2+} which is significant both for Fe_3O_4, FeO and olivine. These phases cannot be distinguished in our measurements. However, it is known that for lower CO_2 concentrations, FeO is thermodynamically favored over Fe_3O_4. The reduction of the Fe_3O_4 crystallites to smaller FeO provides a tentative explanation of the observed decrease in Fe surface content at around 20 vol.% CO_2, preceding the C deposition.

4.2. Carbon

This study provides extensive proof of carbon build-up on the surface of olivine after treatment in CO-containing gas. XRD shows that in addition to the formation of metallic Fe and Fe_3C a significant amount of crystalline graphitic material is formed. This is confirmed by SEM, where carbon fibers can be clearly seen. The carbon formation is most efficient in syngas, followed by water saturated syngas and pure CO. The deposition of carbon on Fe-containing catalysts is a well-known phenomenon and is due to the Boudouard reaction and the CO hydrogenation reaction [31,32].

$$2CO \overset{\text{yields}}{\longrightarrow} CO_2 + C_{solid} \quad (2)$$

$$CO + H_2 \overset{\text{yields}}{\longrightarrow} H_2O + C_{solid} \quad (3)$$

In pure CO, Eq. (2) represents the only possible source of deposited carbon, while in syngas both reactions are possible. The latter of the two reactions have been found to be the faster source of carbon deposition on Fe [31]. Thus the results found here with carbon build-up being fastest in dry syngas and slowest in pure CO are not surprising.

From the experiments with varying compositions of CO_2/CO (see Figs. 7 and 8) it is clear that carbon deposition is preceded by reduction of Fe^{2+} to Fe^0. This is in accordance with theoretical and experimental observations [13,32]. It is also predicted that there is a narrow interval in gas composition where metallic Fe is stable but carbon-deposition is not yet thermodynamically allowed. Furthermore, Nordgreen et al. [13] showed that tar cracking on Fe-based catalysts is significantly more efficient on metallic Fe than on oxides. However, carbon-deposition by decomposition of CO and/or H_2 at too reducing conditions is of course unwanted in a practical application. Therefore, our results suggest that the optimum gas composition, under which Fe_3O_4 reduction starts but carbon-deposition is still suppressed, is between 15 and 20 vol.% CO_2, in a CO_2/CO mixture at 750 °C.

The experiments where the catalyst was first treated in CO-containing gas (resulting in carbon-deposition), followed by oxidation (see Figs. 10 and 11) show that deposited carbon is quickly combusted. For the syngas-treated sample, where the surface is almost completely covered in carbon, about one third of the deposited carbon is removed already after one minute. After 10 min the carbon-level is back at what it was before deposition. For the experiments where samples were repeatedly exposed to cycles of O_2 followed by CO, no build-up of carbon is observed showing that the carbon deposited during CO exposure is rapidly and completely combusted by the subsequent oxidation step.

4.3. Magnesium

The small quantities of MgO in the material, observed with XRD (Figs. 2 and 3), stem either from natural impurities in the mineral or from the high temperature pre-treatment. At the temperature used in this study, no MgO formation is expected. However, we observe that the samples that were not exposed to any gases at all (except for air at room temperature) or that were exposed to water containing gas at 750 °C, contain the smallest amounts of MgO. This could be due to the formation/decomposition of a magnesium hydroxide or oxalate in the presence/absence of water [33]. We have not pursued this observation further, but would like to point it out as an interesting follow-up of this work. Especially since presence of MgO is usually not discussed in the context of olivine, although it is also present in dolomite, another mineral frequently applied as a tar cracking catalyst in biomass gasification [7,34].

It should also be mentioned that the Mg-content at the surface, as measured by XPS, is consistently underestimated compared to the bulk composition. This appears to be due to an inconsistency in the Wagner sensitivity-factors, rather than due to any real effect. However, it does not influence the observed trends, merely the absolute content of the element on the surface.

5. Concluding remarks

There are several important consequences of these observations for the performance of olivine as a catalyst in biomass gasification. The discussion below will predominantly concern dual fluidized bed reactors, where the bed material/catalyst is continuously circulated from a combustor to a gasifier and back again. The residence time in the combustor and gasifier is typically on the time scales from a few seconds to several tens of minutes.

Supported FeOx-catalyst: Olivine is not a stable material during conditions typically applied in biomass gasification. It decomposes during high temperature treatment, forming a mixture of olivine and free FeO_x-phases. The material is thus better regarded as a

FeO_x-catalyst, supported on Mg_2SiO_4 and amorphous SiO_2, than as a homogeneous material.

Oxygen transport: The presence of significant amounts of free Fe-oxide phases allows for oxygen transport from the combustor into the gasifier, thereby facilitating partial combustion of the biomass and/or product gases. In our experiments we see that the Fe_2O_3 and Fe_3O_4 phases can be completely reduced within 1 h. An upper limit to the oxygen transport can thus be estimated as follows: with the material composition corresponding to $(Mg_{0.93}, Fe_{0.07})_2SiO_4$, as calculated from elemental analysis [9], the molar fraction of Fe is 2%. If half of this Fe is present as free, reducible material and if all of it is reduced from Fe_2O_3 to metallic Fe this would correspond to oxygen transport on the order of 1.5 mol% of the bed material or about 1 wt.%. With bed material and biomass feeds of 6300 kg/h and 160 kg/h respectively, as reported in [2] this gives a contribution of 63 kg oxygen per 160 kg biomass in the gasifier. However, the oxygen transport can be limited by conditioning the gas in the gasifier and/or in the combustor or by controlling the residence time in the two chambers, thereby avoiding complete oxidation and reduction.

Fe-phases and catalytic activity: Several studies point to Fe as the catalytically active element in olivine [3,13]. However, different Fe-phases catalyze different reactions. Fe_2O_3 is reported to catalyze soot and NO_x conversion [35], Fe_3O_4 is known as a good water gas shift catalyst [32], FeC is suggested as the active component in Fischer–Tropsch catalysis [36,37] and metallic Fe is known to catalyze the Boudouard reaction and tar decomposition [13,32]. Therefore, the fast change in the oxidation state of the surface Fe will dramatically influence the catalytic properties of the material. Our measurements demonstrate that when an olivine catalyst leaves the combustor, the surface-Fe is present as Fe_2O_3. Upon entering the gasification zone it quickly adapts to the new gas environment. The chemical state of the surface-Fe in a practical situation will critically depend on the gas composition and temperature in the gasifier (thermodynamics). Hence, during the presence in the gasifier the catalytic properties of the catalyst will change accordingly. Whether the material reaches thermodynamic equilibrium, or is kinetically hindered to do so, depend on the temperature and residence time in the gasifier. Therefore, by conditioning the gas mixtures both in the combustor and in the gasifier the catalytic activity could be vastly changed. In addition, steady state measurements of the activity of an olivine catalyst for tar cracking may be quite misleading if the results are applied to dual fluidized bed reactors, were the residence time in the gasifier is short.

Carbon build-up: At the extreme end of catalyst reduction, carbon build-up on the surface is observed. In this state, the catalyst actually contributes to the destruction of the product gases. Furthermore, build-up of graphitic carbon on the surface can deactivate the catalyst for tar cracking by covering the active Fe. This once again points to the importance of properly conditioning the gas composition in the gasifier. However, even if graphitic carbon is formed during gasification, this is quickly combusted in air and regeneration of the catalyst is not a problem.

Acknowledgments

The authors would like to acknowledge Tiny Verhoeven and Marcel Vliex for valuable help with experimental work. Christiaan van der Meijden and Rian Visser at the energy research centre of the Netherlands, for valuable discussions over the addressed questions and interpretation of the results. Use of the Advanced Photon Source, an office of science user facility for the U.S. department of energy (DOE) office of science by Argonne national laboratory, was supported by the U.S. DOE under contract No. DE-AC02-06CH11357 MRCAT operations are supported by the department of energy and the MRCAT member institutions. We acknowledge funding from the European Graduate School on Sustainable Energy and the Advanced Dutch Energy Materials Innovation Lab.

References

[1] F. Kirnbauer, H. Hofbauer, Energy and Fuels 25 (2011) 3793–3798.
[2] C.M. van der Meijden, H.J. Veringa, B.J. Vreugdenhil, B. van der Drift, International Journal of Chemical Reactor Engineering 7 (2009) A53.
[3] S. Rapagna, M. Virginie, K. Gallucci, C. Courson, M. Di Marcello, A. Kiennemann, P.U. Foscolo, Catalysis Today 176 (2011) 163–168.
[4] L. Devi, K.J. Ptasinski, F. Janssen, Industrial and Engineering Chemistry Research 44 (2005) 9096–9104.
[5] S. Koppatz, C. Pfeifer, H. Hofbauer, Chemical Engineering Journal 175 (2011) 468–483.
[6] J. Han, H. Kim, Renewable and Sustainable Energy Reviews 12 (2008) 397–416.
[7] L. Devi, K.J. Ptasinski, F. Janssen, S.V.B. van Paasen, P.C.A. Bergman, J.H.A. Kiel, Renewable Energy 30 (2005) 565–587.
[8] J.N. Kuhn, Z.K. Zhao, L.G. Felix, R.B. Slimane, C.W. Choi, U.S. Ozkan, Applied Catalysis B 81 (2008) 14–26.
[9] D. Swierczynski, C. Courson, L. Bedel, A. Kiennemann, S. Vilminot, Chemistry of Materials 18 (2006) 897–905.
[10] M. Virginie, C. Courson, D. Niznansky, N. Chaoui, A. Kiennemann, Applied Catalysis B 101 (2010) 90–100.
[11] J. Pecho, T.J. Schildhauer, A. Sturzenegger, S. Biollaz, A. Wokaun, Chemical Engineering Science 63 (2008) 2465–2476.
[12] L. Devi, M. Craje, P. Thune, K.J. Ptasinski, F. Janssen, Applied Catalysis A 294 (2005) 68–79.
[13] T. Nordgreen, V. Nemanova, K. Engvall, K. Sjostrom, Fuel 95 (2011) 71–78.
[14] U. Nitsan, Journal of Geophysical Research 79 (1974) 706–711.
[15] C.D. Wagner, Journal of Electron Spectroscopy and Related Phenomena 32 (1983) 99–102.
[16] H. Seyama, M. Soma, Journal of the Chemical Society: Faraday Transactions I 81 (1985) 485–495.
[17] P. Thune, P. Moodley, F. Scheijen, H. Fredriksson, R. Lancee, J. Kropf, J. Miller, J.W. Niemantsverdriet, Journal of Physical Chemistry C 116 (2012) 7367–7373.
[18] T. Yamashita, P. Hayes, Applied Surface Science 254 (2008) 2441–2449.
[19] A.P. Grosvenor, B.A. Kobe, M.C. Biesinger, N.S. McIntyre, Surface and Interface Analysis 36 (2004) 1564–1574.
[20] C.S. Kuivila, J.B. Butt, P.C. Stair, Applied Surface Science 32 (1988) 99–121.
[21] F. Bonnet, F. Ropital, Y. Berthier, P. Marcus, Materials and Corrosion-Werkstoffe und Korrosion 54 (2003) 870–880, http://onlinelibrary.wiley.com/journal/10.1002/%28ISSN%291521-4176
[22] J.N. Kuhn, Z.K. Zhao, A. Senefeld-Naber, L.G. Felix, R.B. Slimane, C.W. Choi, U.S. Ozkan, Applied Catalysis A 341 (2008) 43–49.
[23] R. Dohmen, H.W. Becker, E. Meissner, T. Etzel, S. Chakraborty, European Journal of Mineralogy 14 (2002) 1155–1168.
[24] R. Dohmen, H.W. Becker, S. Chakraborty, Physics and Chemistry of Minerals 34 (2007) 389–407.
[25] D.L. Kohlstedt, J.B. Vandersande, Contributions to Mineralogy and Petrology 53 (1975) 13–24.
[26] L.E. Mayhew, S.M. Webb, A.S. Templeton, Environmental Science and Technology 45 (2011) 4468–4474.
[27] H. Nagahara, I. Kushiro, B.O. Mysen, Geochimica et Cosmochimica Acta 58 (1994) 1951–1963.
[28] I. Gaballah, S. Elraghy, C. Gleitzer, Journal of Materials Science 13 (1978) 1971–1976.
[29] L. Lemelle, F. Guyot, M. Fialin, J. Pargamin, Geochimica et Cosmochimica Acta 64 (2000) 3237–3249.
[30] S. Massouh, A. Perez, J. Serughetti, Physical Review B 33 (1986) 3083–3089.
[31] F. Geurts, A. Sacco, Carbon 30 (1992) 415–418.
[32] C. Ratnasamy, J.P. Wagner, Catalysis Reviews: Science and Engineering 51 (2009) 325–440.
[33] J.A. Wang, O. Novaro, X. Bokhimi, T. Lopez, R. Gomez, J. Navarrete, M.E. Llanos, E. Lopez-Salinas, Materials Letters 35 (1998) 317–323.
[34] E. Gusta, A.K. Dalai, A. Uddin, E. Sasaoka, Energy and Fuels 23 (2009) 2264–2272.
[35] S. Kureti, K. Hizbullah, W. Weisweiler, Chemical Engineering and Technology 26 (2003) 1003–1006.
[36] J.M. Gracia, F.F. Prinsloo, J.W. Niemantsverdriet, Catalysis Letters 133 (2009) 257–261.
[37] J.W. Niemantsverdriet, A.M. van der Kraan, W.L. van Dijk, H.S. van der Baan, Journal of Physical Chemistry 84 (1980) 3363–3370.